RSC Advances

PAPER

View Article Online
View Journal | View Issue



Cite this: *RSC Adv.*, 2024, **14**, 17306

# Preparation and characterization of amphiphilic, biodegradable, waterborne polyurethanes without using organic solvent and catalyst

Zhihui Yang *

Traditionally, waterborne polyurethanes (WPUs) are prepared using toxic organic solvents and catalysts. These WPUs are non-biodegradable and are buried or incinerated after the expiration date. This has adverse effects on the environment and human health, which limits the applications of WPUs. Herein, a special synthetic method was developed for biodegradable waterborne polyurethane (BWPU) by adding hydrophilic prepolymers into WPU prepolymers without using organic solvents and catalysts. Different proportions of polyethylene glycol (PEG) were introduced into polycaprolactone (PCL)-based BWPUs to improve the comprehensive properties. Results showed that as the PEG content was increased from 0 to 16 wt%, the solid content of BWPU increased from 34.8 wt% to 53.1 wt%, while the tensile strength and Young's modulus of BWPU films increased from 21.81 MPa to 56.83 MPa and 8.08 MPa to 19.4 MPa, respectively. However, the elongation at break did not decrease significantly, but still reached 827.17%. With an increase in PEG content, the crystallinity and phase separation decreased, while the hydrophilicity and surface energy increased for BWPU films. In addition, the prepared BWPUs had good biodegradability in PBS/lipase solution. The mass loss of BWPU without PEG reached 6.3 wt% after 4 weeks of degradation, whereas the mass losses of BWPUs with PEG reached 2.3–4.3 wt%. Obviously, the introduction of PEG did not increase biodegradability. Thus, the higher the PCL content, the faster the biodegradation rate. This work would provide an effective method for the preparation of ecofriendly biodegradable BWPU with excellent comprehensive properties.

Received 17th March 2024
Accepted 22nd May 2024

DOI: 10.1039/d4ra02044h

rsc.li/rsc-advances



## 1. Introduction

Currently, the demand for degradable, biocompatible, and biofunctional polymer materials has increased, especially in temporary therapeutic applications, such as drug delivery systems, surgical sutures, tissue engineering scaffolds, *etc.*[1,2] In addition, due to the increase in plastic waste year by year, degradable polymers have become attractive for environmental applications.[3,4]

Polyurethane (PU) is one of the polymeric materials most widely used in coatings, inks, adhesives, and foams, due to its excellent combination of properties, such as chemical resistance, flexibility, and mechanical and adhesive properties.[5–7] However, several organic solvents, including toluene, xylene, formaldehyde, *etc.*, are used in PU synthesis, which seriously pollute the environment and endanger human health.[8,9] In contrast, water-based polyurethane (WPU) that uses water as the solvent, is more environment-friendly and also retains the remarkable properties of solvent-based PU, such as molecular structure designability as well as excellent mechanical and adhesion properties.[10] It is important to note that traditional WPU is non-biodegradable.

Biodegradable materials can be categorized as natural and synthetic materials on the basis of their source.[11] Natural materials exhibit antibiosis, biocompatibility, and biodegradability; however, their mechanical properties are poor.[12,13] Travinskaya *et al.*[14] prepared a starch-containing aqueous anionic polyurethane dispersion (APU/St) by introducing aqueous starch solution into anionic WPU solution. Results showed that the prepared APU/St films were more susceptible to alkaline and acidic hydrolysis and the tensile strengths of the films could reach only 2.4–8.7 MPa. Dai *et al.*[15] first synthesized soybean oil-based polyols using epoxy soybean oil and ricinoleic acid as the raw materials. These polyols were then reacted with isophorone diisocyanate and dimethylol propionic acid to obtain oil-based waterborne polyurethanes (SWPU) with different *R* values (*R* value represents the molar ratio of –NCO/–OH). Results showed that when the *R* value of SWPU was increased from 1.1 to 1.4, the tensile strength of SWPU films increased from 10.02 MPa to 27.32 MPa, and the initial decomposition temperature increased from 201 °C to 246 °C. Further, after degradation for 24 h the SWPU films experienced weight losses of 35.77–31.39%. Therefore, in the study, although SWPU had good degradability, its maximum tensile

*Qinghai Key Laboratory of Advanced Technology and Application of Environmental Functional Materials, Department of Chemistry, Qinghai Normal University, Xining, 810016, P. R. China. E-mail: 446920348@qq.com; Tel: +86-971-6303132*

strength could reach only 27.32 MPa. Lee *et al.*[16] prepared a series of biodegradable WPU/gelatin hybrids. Cold fish gelatin was introduced into WPU through covalent bonding to increase the biodegradability of the materials. Results showed that when chemically modified gelatin was introduced into the WPU hybrids, the water resistance, hardness, and glassy state modulus of the WPU hybrids increased, but the tensile strength and elongation at break could reach only 14.6–16.6 MPa and 201.4–370.0%, respectively. The above examples indicated that although the use of some natural materials could increase the biodegradability of WPU, it caused a decline in the mechanical properties of WPU. However, it is crucial for biodegradable materials to possess good mechanical properties for applications in specialty fields, such as tissue engineering.[17]

Synthetic polymers can be easily tailored, designed and chemically modified, as compared to natural polymers. In view of this, the synthesis, characterization, commercialization, and application of biodegradable synthetic polymers have received extensive attention.[18,19] Polycaprolactone (PCL) is a multipurpose biodegradable synthetic polymer having glass transition temperature of −60 °C and melting point of 60 °C. In general, its introduction into polymeric materials as an additive improves their properties and applications. For example, introduction of PCL as a polyol component in PU renders PU resistant to especially oil, organic solvents, water, and chlorine.[20,21] In addition, PCL is a semi-crystalline and water-insoluble polymer, which becomes biodegradable due to the hydrolysis of ester bonds. Hence, PCL itself and its derivatives, especially its composites, are widely used in biodegradable and anti-corrosion formulations.[22,23]

WPU can be easily made biodegradable by introducing biodegradable components, such as ester-based diols into the soft segments of WPU.[24] As mentioned above, the introduction of PCL into WPU can improve the biodegradability of WPU and also enhance its mechanical properties. This has more advantages as compared to the introduction of natural materials into WPU to improve degradability. However, ester-based diol is prone to degradation by hydrolysis, even over short periods of time, which limits their applications in certain fields, such as tissue engineering.[25] Therefore, in the exploration of more biostable materials, ether-based polyols have been used in the preparation of WPU. Polyethylene glycol (PEG) is a linear polyether widely used in many industrial, manufacturing, biological, and pharmaceutical applications.[26] PEG is inherently non-biodegradable, since its –C–C–bond is quite resistant to microbial degradation. However, PEG can undergo biodegradation in some specific oxidative environments and can also be excreted from the body through the kidneys. In general, PEG and its derivatives are recognized as low cost, non-toxic, and environment-friendly derivatives with high biocompatibility.[27,28]

In this work, a series of biodegradable waterborne polyurethanes (BWPUs) were synthesized by a special method of adding hydrophilic prepolymers into WPU prepolymers without adding organic solvents and catalysts. A mixture of PCL and PEG were used as a soft segment and *N*-[(2-aminoethyl)-amino] ethane sulfonated sodium was used as post-chain extender. The effects of PEG content on the particle size, thermal properties, dynamic mechanical properties, mechanical properties, surface properties, and biodegradability of BWPUs were investigated. This work would serve as a theoretical reference for the solvent-free, catalyst-free synthesis of biodegradable polymer materials with excellent comprehensive properties.

## 2. Experimental

### 2.1 Materials

Polycaprolactone diol (PCL, $M_n$ = 2000, Maikelin, China) and poly (ethylene glycol) (PEG, $M_n$ = 2000, Maikelin, China) were dried at 80 °C under vacuum for 8 h. Isophorone diisocyanate (IPDI, 98% purity, Aladdin), dimethylol propionic acid (DMPA, 99% purity, China), triethylamine (TEA, AR grade, Maikelin, China), and *N*-[(2-aminoethyl)-amino] ethane sulfonated sodium (AAS, AR grade, Taiwan, China) were used as received.

### 2.2 Synthesis of BWPU dispersions

**2.2.1 Preparation of hydrophilic prepolymer A.** The composition of hydrophilic prepolymer A is presented in Table 1, wherein the PEG/IPDI/DMPA constituents were in molar ratio of 1 : 3 : 0.5. The entire amount of PEG and certain amount of IPDI were added to the reactor under nitrogen and mechanically stirred. The mixture was stirred at 55 °C for 15 min to obtain a homogeneous solution. The reaction temperature was then raised to 85 °C and held for 90 min. Subsequently, the reaction was cooled to 80 °C, and certain amount of DMPA was added to the reaction system. The reaction was continued until the NCO content of prepolymer reached the theoretical value and the reaction was ceased to obtain the hydrophilic prepolymer A.

**2.2.2 Preparation of BWPU dispersions and films.** The compositions of BWPU dispersions are presented in Table 1. The NCO/(OH + NH) molar ratio was defined by the *R* value,

Table 1 Composition of BWPU dispersions

| | | | Hydrophilic prepolymer A | | | | | | |
|---|---|---|---|---|---|---|---|---|---|
| Sample | PCL (g) | IPDI (g) | PEG (g) | IPDI (g) | DMPA (g) | DMPA (g) | TEA (g) | AAS (g) | wt% of PEG as soft segment |
| BWPU0 | 25 | 9.770 | 0 | 0 | 0 | 1.324 | 0.979 | 1.730 | 0 |
| BWPU1 | 15 | 5.936 | 1.300 | 0.433 | 0.043 | 0.771 | 0.647 | 1.128 | 8 |
| BWPU2 | 15 | 6.191 | 2.850 | 0.949 | 0.095 | 0.748 | 0.707 | 1.353 | 16 |
| BWPU3 | 15 | 6.038 | 4.737 | 1.577 | 0.158 | 0.723 | 0.783 | 1.322 | 24 |
| BWPU4 | 15 | 6.206 | 7.060 | 2.350 | 0.236 | 0.688 | 0.875 | 1.505 | 32 |

where $R$=NCO(IPDI)/[OH(PCL + PEG + DMPA) +NH(AAS)] was set as 1.4 for all BWPUs. In the preparation of BWPU, the mass percentage of PEG ($W_{PEG}$) in the soft segments was changed. The $W_{PEG}$ of prepared BWPU were 0, 8 wt%, 16 wt%, 24 wt%, and 32 wt% and the corresponding BWPU samples were named BWPU0, BWPU1, BWPU2, BWPU3, and BWPU4, respectively.

PCL and the rest of IPDI were added to a four-necked flask, equipped with nitrogen inlet, condenser, and mechanical stirrer, and heated to 85 °C and held for 90 minutes. The hydrophilic prepolymer A and the rest of DMPA were added into the reaction system till the NCO content of the system reached the theoretical value and the temperature was lowered to 50 °C. TEA was added to the reaction system over a period of 30 minutes, and the BWPU prepolymer was obtained. Subsequently, metered amounts of deionized water were added to the prepared BWPU prepolymer under high speed stirring at 1000 rpm. Meanwhile, AAS was dropped into the dispersed system and reacted for 30 minutes to finally obtain BWPU dispersions with high solids contents of 50.8–53.1 wt%. Scheme 1 shows the route for the preparation of BWPU dispersions and films. BWPU films were obtained by pouring BWPU dispersions into polytetrafluoroethylene mold, drying them at room temperature for 24 hours, and then shifting them to a vacuum drying oven at 70 °C and keeping them until the films reached constant weight.

### 2.3 Material characterization

**2.3.1 Solids content determination.** The solids contents of BWPU dispersions were determined by weighing the sample before and after water evaporation. Approximately 2 g of the BWPU dispersion was poured into a glass dish, which was then transferred to an oven and the water was evaporated at 100 °C until a constant weight was achieved. The solids content of each sample was calculated as the average of three experiments.

**2.3.2 Average particle size analysis.** The average particle sizes of BWPU dispersions were measured using a laser particle size analyzer (Brookhaven 90 plus, Germany) at room temperature. The BWPU dispersions were diluted to approximately 0.5% in deionized water prior to analysis.

*2.3.2.1 Attenuated total reflectance-fourier transform infrared spectroscopy (ATR-FTIR).* The structures of BWPU were characterized using ATR-FTIR spectrometer (IS50, Nicolet, USA) at a resolution of 4 $cm^{-1}$ and 64 number of scans.

**2.3.3 Differential scanning calorimetry (DSC).** The thermal properties of the BWPU were determined using a differential scanning calorimeter (PerkinElmer, USA). The heating rates for the first and second runs were 10 °C $min^{-1}$ and the cooling rate

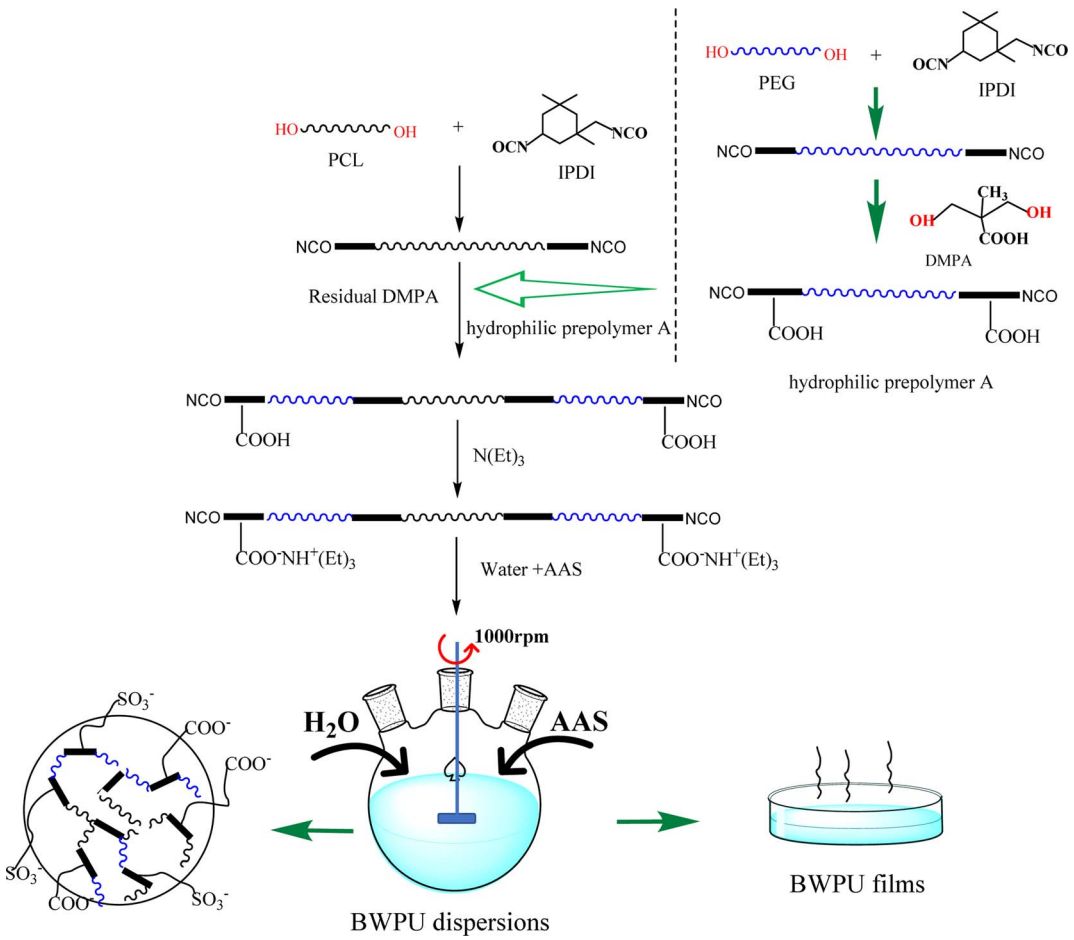


Scheme 1 Route for the preparation of BWPU dispersions and films.

was 5 °C $min^{-1}$. All the tests were conducted in a nitrogen atmosphere.

**2.3.4 Dynamic mechanical analysis (DMA).** The dynamic mechanical properties of BWPU were tested using a dynamic mechanical analyzer (PerkinElmer USA). The test was performed at 10 Hz, 5 °C $min^{-1}$, and the temperature range was −90 °C to 100 °C.

**2.3.5 Tensile property testing.** The tensile properties of BWPU were tested using an electronic tensile tester (Instron, USA). BWPU sample was cut to specimen sizes of 30 mm × 4 mm × 1 mm and the testing was conducted at a crosshead speed of 50 mm $min^{-1}$.

**2.3.6 Water contact angle measurements.** The water contact angle of BWPU was tested using a contact angle tester (DSA 30, Kruss, Germany). The thickness of each sample film was approximately 1 mm. Each BWPU film was tested thrice by dropping deionized water on the film surface.

**2.3.7 Biodegradability testing.** The BWPU films were cut to specimen sizes of 10 mm × 10 mm × 1 mm and were placed in a 100 mL capped tube containing 50 mL of degradation buffer including phosphate buffer solution (PBS) (pH = 7.4) and lipase (200 U $mL^{-1}$) in a volume ratio of 4 : 1. At different time periods during degradation, the sample was collected and washed three times with distilled water and then transferred to a vacuum oven and dried at 50 °C till constant weight.

# 3. Results and discussion

## 3.1 Characterization of BWPU dispersions

The properties of BWPU dispersions were determined for their practical applications. Some key properties of BWPU dispersions are listed in Table 2. It was evident that the solids content of BWPU dispersions containing PEG was significantly higher than that without PEG (BWPU0). BWPU2 had the highest solids content of 53.1%. Further, particle size and particle size distribution are also important indexes to evaluate the properties of BWPU dispersions.[29] Fig. 1 shows particle sizes and particle size distributions of the BWPU dispersions with different $W_{PEG}$. With an increase in PEG content, both particle size and particle size distribution of BWPUs decreased initially and then increased. When $W_{PEG}$ was 16%, BWPU2 had the smallest particle size and polydispersity index (214.32 nm and 0.1, respectively). When $W_{PEG}$ increased to 24% and 32%, the particle sizes and polydispersity indexes of the BWPU3 and BWPU4 increased to 220.65 nm and 357.00 nm and 0.135 and 0.284, respectively. This could be attributed to the fact that with

Table 2 Properties of BWPU dispersions

| Sample | Solid content (wt%) | Average particle size (nm) | Polydispersity index | Storage stability |
|---|---|---|---|---|
| BWPU0 | 34.8 | 440.52 | 0.263 | >6 months |
| BWPU1 | 51.4 | 354.10 | 0.242 | >6 months |
| BWPU2 | 53.1 | 214.32 | 0.100 | >6 months |
| BWPU3 | 51.6 | 220.65 | 0.135 | >6 months |
| BWPU4 | 50.8 | 357.00 | 0.284 | >6 months |

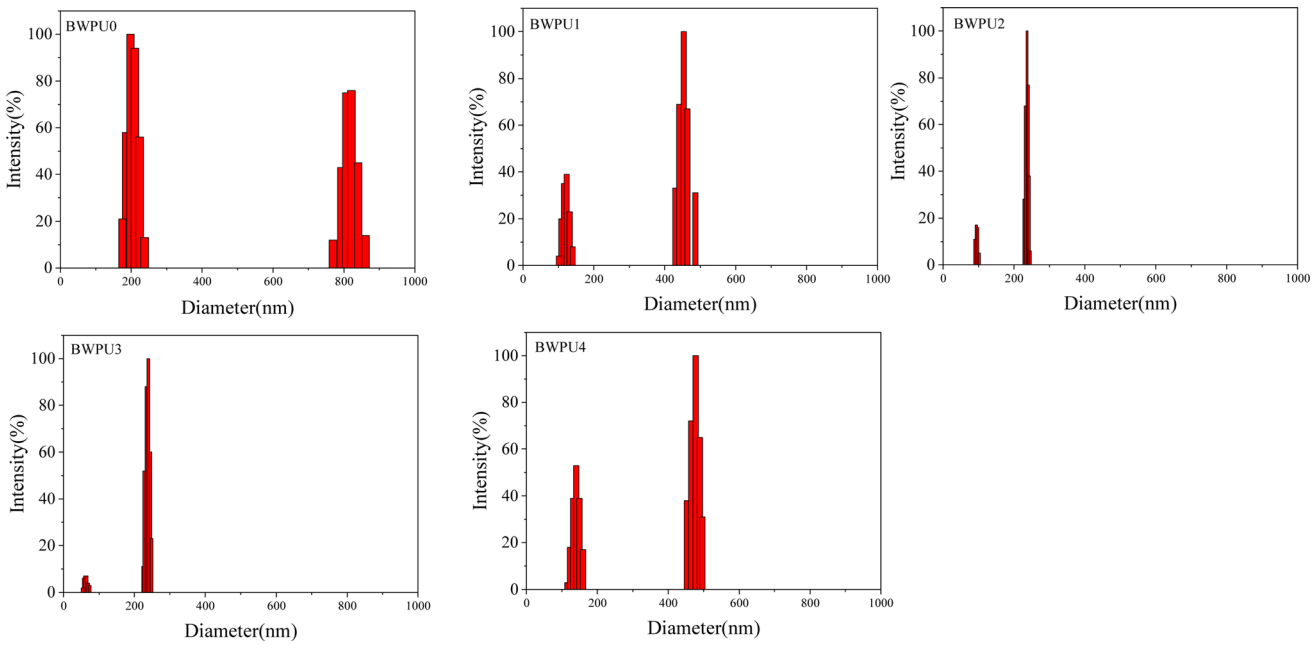


Fig. 1 Particle sizes and particle size distributions of BWPU dispersions with different $W_{PEG}$.

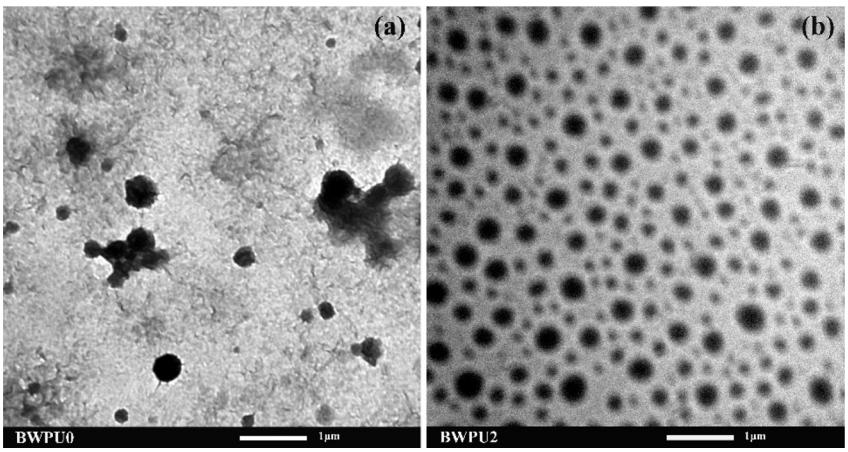


Fig. 2 TEM images of BWPU0 (a) and BWPU2 (b) dispersions.

an increase in $W_{PEG}$, more hydrophilic chains got embedded into the water, forming a dense hydrated layer. In contrast to this, these hydrophilic segments could not enter the surfaces of the latex particles. This made it more difficult for the latex particles to attain smaller particle sizes and distribution.[30] Fig. 2(a and b) show the TEM images of BWPU0 and BWPU2 dispersions, respectively. The latex particles of BWPU2 dispersions containing 16% of PEG were individually separated and more evenly distributed. This could be attributed to the introduction of PEG that increased the hydrophilicity and flexibility of the hydrophobic BWPU macromolecular chains, thereby increasing the dispersibility of BWPU. The number of latex particles in BWPU0 dispersions was less and some of them formed clusters that increased the average particle size and broadened the particle size distribution of BWPU dispersions. Therefore, it was evident that BWPU2 dispersions had the best comprehensive properties.

### 3.2 Structure and phase separation of the BWPU films

Infrared spectroscopy characterizes the chemical structure and phase separation of hard and soft segments in BWPUs.[25] Fig. 3(a and b) show ATR-FTIR spectra of BWPU films with different $W_{PEG}$ and the consumption of IPDI monomer of BWPU2 sample at different reaction times, respectively. From Fig. 3(a), the peaks at 3336 $cm^{-1}$ and 1733 $cm^{-1}$ were attributed to the N–H stretching and C=O stretching vibrations, respectively. The peak at 2855–2955 $cm^{-1}$ was attributed to the C–H stretching vibrations. The peak at 1105 $cm^{-1}$ was ascribed to the C–O–C bonds of PEG. The BWPU0 sample without PEG showed no peak at 1105 $cm^{-1}$, whereas the other four BWPU samples that contained PEG showed the presence of this peak. This confirmed the successful introduction of PEG into the BWPU structure. In Fig. 3(b), the peak at 2265 $cm^{-1}$ was attributed to the –NCO stretching vibrations. The intensity of –NCO decreased as the reaction time increased. The peak disappeared completely when the reaction time reached 7 h, which essentially indicated the completion of reaction of –NCO. Further, the peaks at 3336 $cm^{-1}$ and 1535 $cm^{-1}$ corresponded to the stretching and bending vibrations of N–H, respectively. It was evident that the intensity of these peaks increased with increase in reaction time. This result suggested that the soft and hard segments reacted to form more number of carbamate and urea bonds.[31,32]

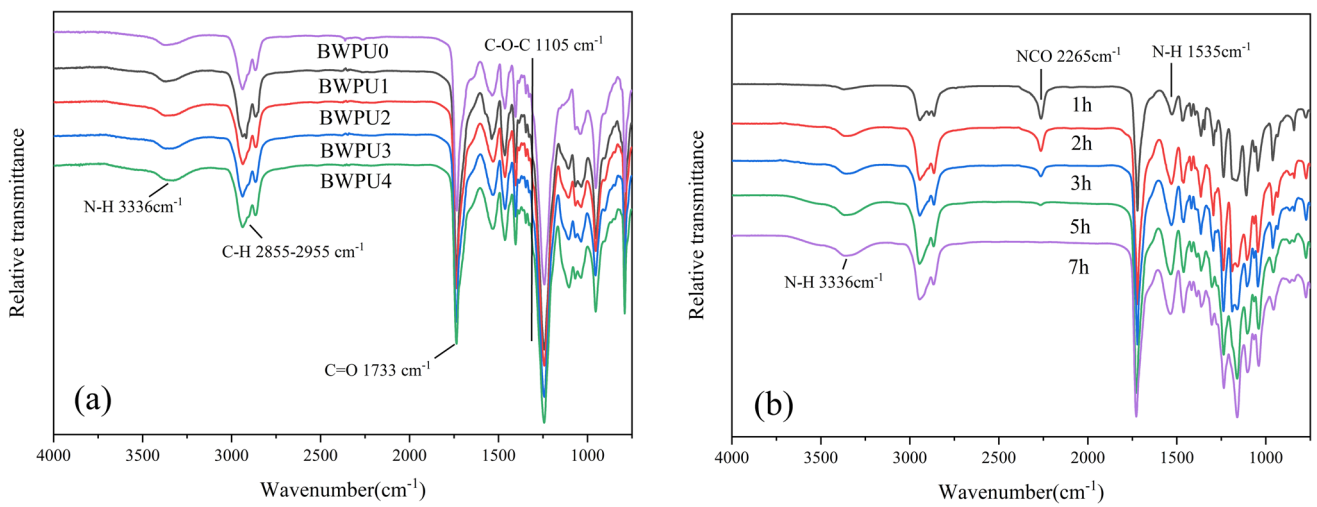


Fig. 3 ATR-FTIR spectra of (a) BWPU films with different $W_{PEG}$ and (b) consumption of IPDI monomer of BWPU2 sample different reaction times.

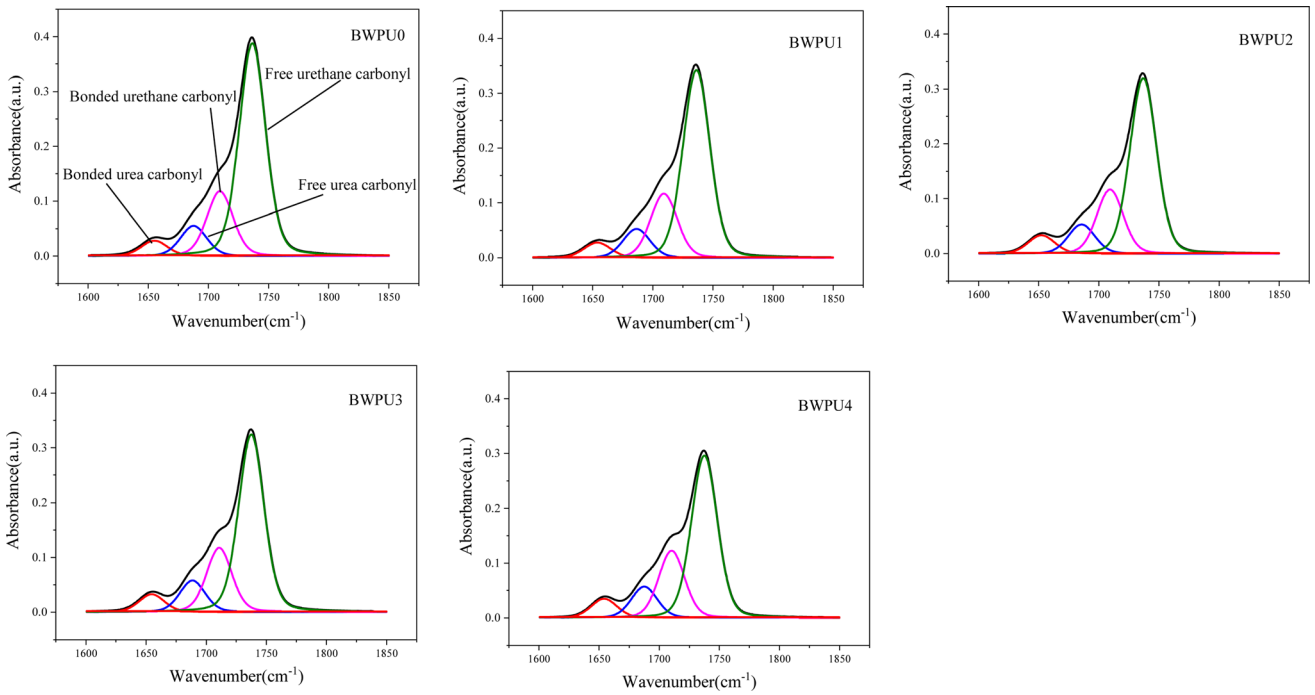


Fig. 4 Deconvoluted peaks of C=O stretching vibrations in the FTIR spectra of the BWPU with different $W_{PEG}$.

Further, Fig. 4 shows the deconvoluted peaks of C=O stretching region in the FTIR spectra of the BWPUs and Table 3 presents the relevant data. The hydrogen bonding index (HBI) is often used to determine the degree of hydrogen bonding and is defined by formula (1):[33]

$$\mathrm{HBI} = A(\text{bonded C=O})/A(\text{free C=O}) \quad (1)$$

where, $A$(bonded C=O) and $A$(free C=O) are the peak areas of bonded C=O and free C=O, respectively. Table 3 shows the calculated HBI values of the BWPUs. Generally, the higher the value of HBI, the greater is the degree of phase separation of hard and soft segments in WPU.[34] From Table 3, it was clear that compared with other BWPU samples containing PEG, the HBI value of the BWPU0 was the highest, and therefore its degree of phase separation also was maximum. The soft segments in BWPU0 were composed only of PCL and the hydrophobicity of PCL could reduce the compatibility between hard and soft segments. In addition, the HBI value of BWPU1 to BWPU4 gradually decreased, indicating that their degree of phase separation gradually decreased.

### 3.3 Thermal properties of BWPU films

DSC is used to analyze the thermal properties of BWPU films.[35] Fig. 5 shows the DSC thermograms of BWPU films and pure PCL during heating and cooling processes and Table 4 lists the relevant data. Generally, the melting peak of PEG component is 35–36 °C, whereas the melting peak of PCL about 45–50 °C in WPU.[36] In Fig. 5(a), only one melting peak of PCL appeared at 45–50 °C, whereas there was no obvious melting peak of PEG. This was ascribed to the low molecular weight of PEG and lower mass fraction in the PEG/PCL soft segment. In the first heating scan, pure PCL showed higher melting temperature ($T_m$) and melting enthalpy ($\Delta H_m$) than all BWPU samples. Of the four BWPU samples containing PEG, BWPU1 had the highest $T_m$ (43.7 °C) and $\Delta H_m$ (23.2 J g$^{-1}$). In addition, the degree of crystallinity ($\alpha_c$) of BWPUs could be calculated using formula (2):[37,38]

$$a_{\mathrm{cBWPU}}\% = 100 \times \Delta H_{\mathrm{BWPU}}/\Delta H_{\mathrm{PCL}} \times (\mathrm{wt}\%_{\mathrm{PCL}}) \quad (2)$$

Table 3 HBI values from the C=O peaks in FTIR spectra

| | Peak position (cm$^{-1}$) | | | | Peak area | | | | |
|---|---|---|---|---|---|---|---|---|---|
| Sample | Bonded urea | Free urea | Bonded urethane | Free urethane | Bonded urea | Free urea | Bonded urethane | Free urethane | HBI |
| BWPU0 | 1655 | 1688 | 1710 | 1737 | 0.99 | 1.67 | 3.53 | 8.53 | 0.44 |
| BWPU1 | 1656 | 1689 | 1711 | 1737 | 0.95 | 1.66 | 3.58 | 9.37 | 0.41 |
| BWPU2 | 1653 | 1686 | 1709 | 1736 | 0.97 | 1.55 | 3.41 | 9.38 | 0.40 |
| BWPU3 | 1655 | 1687 | 1709 | 1736 | 0.82 | 1.57 | 3.48 | 10.20 | 0.36 |
| BWPU4 | 1655 | 1688 | 1706 | 1736 | 0.83 | 1.64 | 3.52 | 11.56 | 0.32 |

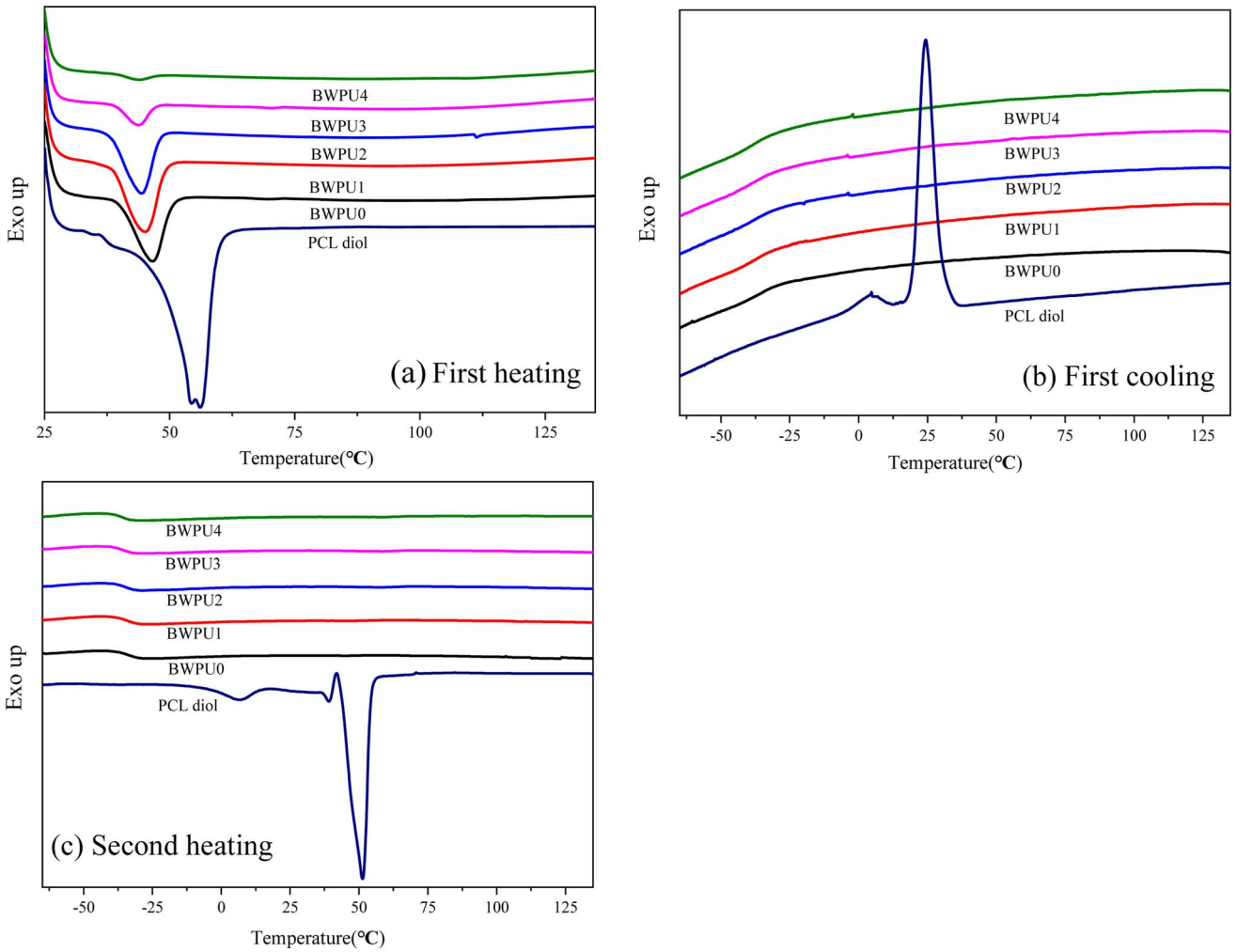


Fig. 5 DSC thermograms of BWPU films with different $W_{PEG}$: (a) first heating scan; (b) first cooling scan; and (c) second heating scan.

where $\Delta H_{BWPU}$ and $\Delta H_{PCL}$ are the melting enthalpies of BWPU and pure PCL, respectively. $wt\%_{PCL}$ is the mass percentage of PCL in BWPU. The $\alpha_c$ of pure PCL was calculated to be 44.3%, based on the $\Delta H_m$ (139.5 J $g^{-1}$) of 100% crystalline PCL. From Table 4, the $\alpha_c$ of BWPUs was found to be lower than that of pure PCL. This was ascribed to the bonding between the hard and soft segments and the impediment in crystallization of PCL in BWPUs due to the introduction of PEG. Among all BWPUs containing PEG, BWPU1 had the highest $\alpha_c$, which was attributed to its lowest PEG content (8 wt%) and maximum phase separation of hard and soft segments in BWPU1 (as confirmed by FTIR analysis). This facilitated the crystallization of PCL more readily. The crystallization behavior of pure PCL was determined during both the first cooling (Fig. 5b) and second heating scans (Fig. 5c). However, the crystalline phases of all BWPUs were not observed during either of the processes. Results indicated that the crystallization efficiencies of PCL soft segments that precipitated from the BWPU dispersions at room

Table 4 Thermal properties of BWPU films and pure PCL as determined by DSC

| | 1st heating (10 °C $min^{-1}$) | | | 2nd heating (10 °C $min^{-1}$) | | | |
|---|---|---|---|---|---|---|---|
| Sample | $T_m$ (°C) | $\Delta H_m$ (J $g^{-1}$) | $\alpha_c$ (%) | $T_{gs}$ (°C) | $T_m$ (°C) | $\Delta H_m$ (J $g^{-1}$) | $\alpha_c$ (%) |
| BWPU4 | 45.3 | 1.9 | 2.7 | −38.5 | — | — | — |
| BWPU3 | 44.1 | 8.7 | 11.1 | −37.2 | — | — | — |
| BWPU2 | 43.5 | 20.1 | 23.2 | −36.0 | — | — | — |
| BWPU1 | 43.7 | 23.2 | 24.5 | −35.8 | — | — | — |
| BWPU0 | 46.6 | 24.3 | 23.4 | −33.3 | — | — | — |
| PCL | 55.1 | 61.8 | 44.3 | — | 51.1 | 50.4 | 36.1 |

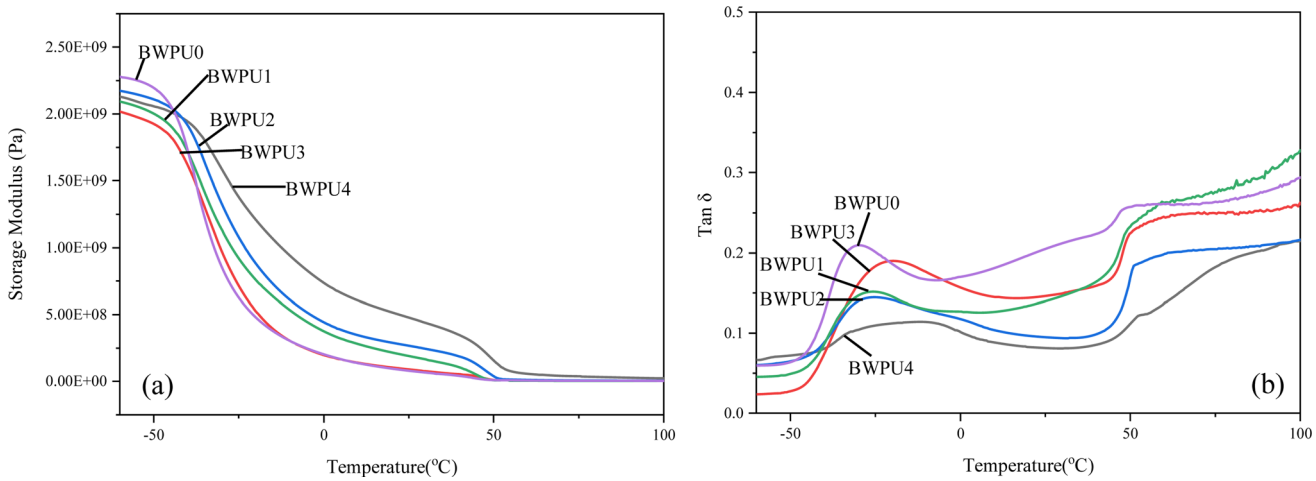


Fig. 6 DMA curves of BWPU films with different $W_{PEG}$: (a) storage modulus, (b) tan $\delta$.

temperature were higher than that of PCL from melting process. Moreover, the glass transition temperatures of the BWPU soft segments ($T_{gs}$) were determined during the second heating scan. The $T_{gs}$ values of five BWPU samples decreased in the order of BWPU0 > BWPU1 > BWPU2 > BWPU3 > BWPU4. As the PEG content was increased, the number of $(-CH_2-CH_2-O-)_n$ chains that were introduced increased, which increased the mobility of the molecular chains, and consequently the $T_{gs}$ value decreased gradually.

### 3.4 Dynamic mechanical properties of the BWPU films

Fig. 6 shows the DMA curves of BWPU films. From Fig. 6(a), it was evident that below −50 °C, all BWPUs were in a glassy state and their storage moduli remained almost unchanged. As the temperature increased, BWPUs entered the zone of glassy transition, after which the storage modulus decreased rapidly. Fig. 6(b) shows two damping peaks in the temperature range of −50 °C to −10 °C and 40 °C to −70 °C, which corresponded to the $T_{gs}$ domains and the glass transition temperatures of the domains with hard segments ($T_{gh}$), which indicated microphase separation of BWPU.[39] Table 5 presents the $T_g$ values of BWPUs determined from the DMA curve. The $T_{gs}$ value was slightly higher than that obtained by DSC, because of the difference in testing environments.[40] In general, the higher the value of $\Delta T_g$ ($\Delta T_g = T_{gh} - T_{gs}$), the more is the phase separation between the soft and hard segments.[41] The $\Delta T_g$ values of five BWPU samples decreased in the order BWPU0 > BWPU1 > BWPU2 > BWPU3 > BWPU4. This indicated that the degree of phase separation was also in this order and the results were consistent with those of infrared analysis.

Table 5 $T_g$ values of BWPUs as determined from the DMA curves

| Sample | BWPU0 | BWPU1 | BWPU2 | BWPU3 | BWPU4 |
|---|---|---|---|---|---|
| $T_{gs}$ (°C) | −31.97 | −29.81 | −27.12 | −23.08 | −21.97 |
| $T_{gh}$ (°C) | 52.13 | 51.97 | 51.93 | 51.91 | 51.75 |
| $\Delta T_g$ (°C) | 84.10 | 81.78 | 79.05 | 77.99 | 73.72 |

### 3.5 Mechanical properties of BWPU films

The mechanical properties of WPU films can be evaluated through tensile testing.[42] The introduction of PEG had a strong impact on the tensile properties of BWPUs. The typical tensile stress–strain curves and the results of tensile testing of BWPUs are shown in Fig. 7 (a and b). The introduced PEG could impart certain flexibility and plasticity to the BWPU films. This rendered the BWPU more flexible and had an effect on its mechanical properties.[43,44] With an increase in PEG content, both the tensile strengths and Young's moduli of the BWPUs first increased and then decreased. When the PEG content was increased from 0 (BWPU0) to 16% (BWPU2), the tensile strength and Young's modulus of BWPU films increased from 21.81 MPa to 56.83 MPa and 8.08 MPa to 19.4 MPa, respectively. However, the elongation at break did not decrease significantly, but still reached 827.17%. This could be due to the fact that BWPU2 had a higher content of hard segments (33.5%) and appropriate degree of phase separation. This increased the cohesive energy and molecular chain flexibility of the BWPU. Therefore, the mechanical properties of BWPU2 were confirmed to be the best among all BWPUs.

### 3.6 Surface properties of BWPU films

The hydrophilic and hydrophobic properties of BWPU films were studied by static water contact angle and water absorption tests at 25 °C. Fig. 8 shows the contact angles and water absorptivities of the five BWPU films. Table 6 lists the relevant data of surface properties. It was evident that water absorptivity increased with an increase in $W_{PEG}$. However, the trend of water contact angle was opposite, wherein the water wettability of BWPU films increased with an increase in $W_{PEG}$.[45] The increase of $W_{PEG}$ in BWPU led to an increase in number of hydrophilic groups (–$CH_2$–$CH_2$-O-). Further, as the hydrophilicity of BWPU films increased, it was easier for water molecules to penetrate and diffuse into the BWPU films.[46,47] Consequently, the water absorption increased and water contact angle decreased with an increase in $W_{PEG}$. Next, the surface energies of the five BWPU

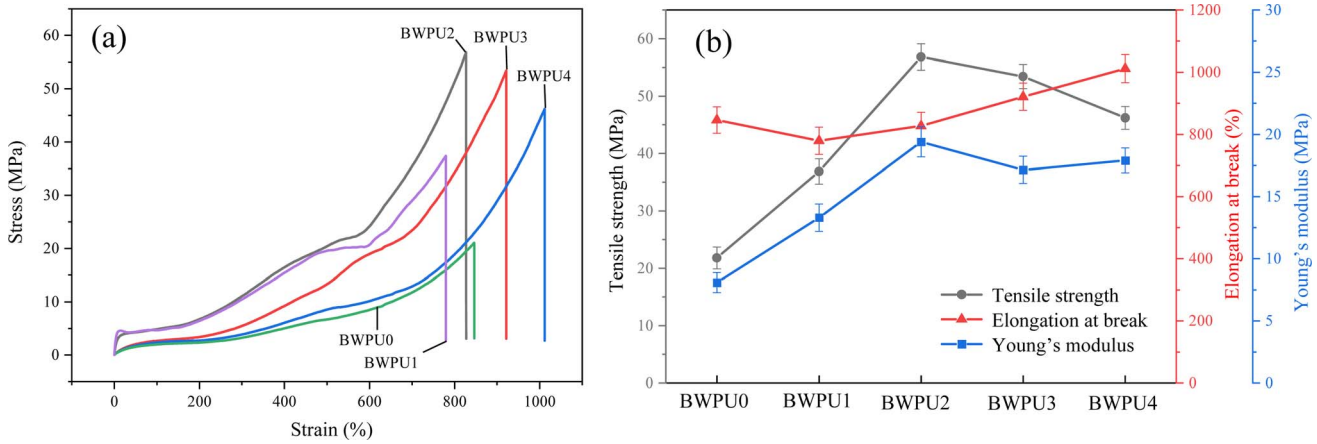


Fig. 7 Tensile stress–strain curves (a) and the results of tensile testing of BWPU films with different $W_{PEG}$ (b).

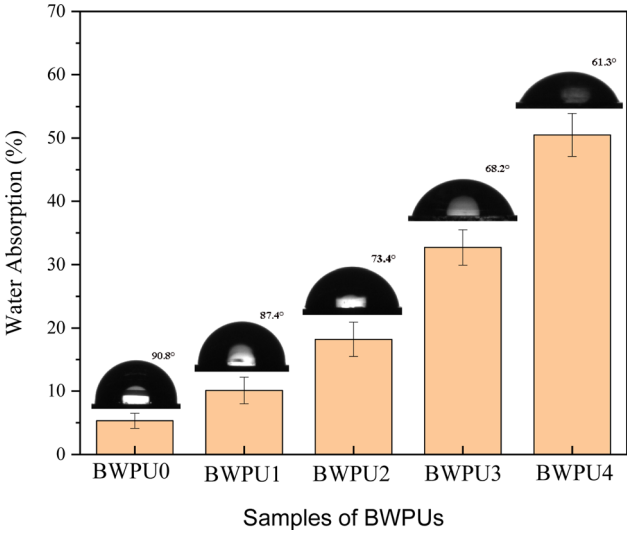


Fig. 8 Contact angles and water absorptivities of BWPU films with different $W_{PEG}$.

films were determined by static contact angle measurements of water and ethylene glycol on BWPU films, and were calculated according to formulae (3) and (4):[48–50]

$$\gamma_L(1+\cos\theta) = 4\left(\frac{\gamma_S^d\gamma_L^d}{\gamma_S^d+\gamma_L^d} + \frac{\gamma_S^p\gamma_L^p}{\gamma_S^p+\gamma_L^p}\right) \quad (3)$$

$$\gamma_s = \gamma_s^d + \gamma_s^p \quad (4)$$

where, $\gamma_L$, $\gamma_s$, $\gamma_s^d$, and $\gamma_s^p$ are the surface tension, surface energy, and the dispersion component and polar components of the solid, respectively; $\gamma_L^d$ and $\gamma_L^p$ are the dispersion component and polar component of the liquid, respectively. The polar component and dispersion component of water are 51.0 mJ $m^{-2}$ and 21.8 mJ $m^{-2}$, respectively, and those of ethylene glycol were 19.0 mJ $m^{-2}$ and 29.3 mJ $m^{-2}$, respectively.

In general, the surface energy of WPU was low and its surface anti-fouling effect was good. However, a low surface energy implied that the adhesion between the two interfaces was low.[51] The surface energies of BWPU films with different $W_{PEG}$ are presented in Table 6. It was evident that from BWPU0 to BWPU4, the contact angle for both water and ethylene glycol decreased with an increase in $W_{PEG}$, whereas the surface energy increased. Soft segments in WPU were more likely to migrate closer to the surface in contact with air.[52] When the PEG content was high, the PCL content was low. In BWPU0 to BWPU4 samples, the percentages of PCL were 64.4%, 59.3%, 53.7%, 49.4%, and 44.2%, respectively. This led to a decrease in the number of polar hydrophobic ester groups of PCL on the surface of BWPU films. Consequently, there was a decrease in the surface energy of BWPU films.[53]

### 3.7 Biodegradability of the BWPU films

Biodegradability of BWPU films was investigated by immersing the BWPU films in PBS/lipase solution for 4 weeks. Fig. 9 shows the degradation profiles of the five BWPU films in PBS/lipase

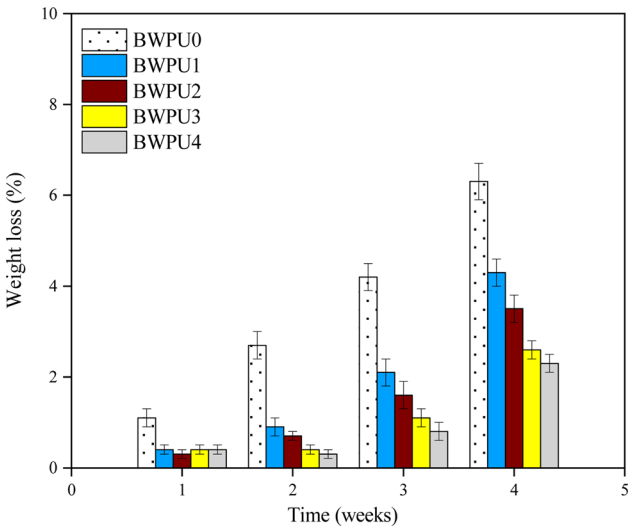


Fig. 9 Degradation profiles of BWPU films over 4 weeks in PBS/lipase solution.

Table 6 The surface properties of BWPU films

| Sample | Water absorption (%) 72 h and 25 °C | Contact angle (°) $H_2O$ | Contact angle (°) $(CH_2OH)_2$ | Surface energy (mJ m$^{-2}$) $\gamma_S^p$ | $\gamma_S^d$ | $\gamma_s$ |
|---|---|---|---|---|---|---|
| BWPU0 | 5.3 | 90.8 | 66.5 | 14.97 | 11.02 | 26.00 |
| BWPU1 | 10.1 | 87.4 | 60.2 | 17.47 | 11.41 | 28.88 |
| BWPU2 | 18.2 | 73.4 | 53.1 | 13.58 | 21.31 | 34.89 |
| BWPU3 | 32.7 | 68.2 | 47.6 | 14.30 | 24.00 | 38.30 |
| BWPU4 | 50.5 | 61.1 | 40.4 | 15.05 | 28.03 | 43.09 |

solution over 4 weeks. All BWPU films showed progressive weight loss over four weeks of degradation in PBS/lipase solution. The degradation rate of the BWPU0 specimen without PEG was obviously the highest, wherein its mass loss reached 6.3% after 4 weeks of degradation. In addition to the first week, the order of degradation rate of the four BWPU samples in 2, 3, and 4 weeks was as follows: BWPU1 > BWPU2 > BWPU3 > BWPU4. PCL could be degraded by lipase, so lipase interacted only with the PCL soft segments in BWPU. From BWPU0 to BWPU4, the percentage of PCL in BWPU decreased gradually. Therefore, it could be concluded that the biodegradation rate of all BWPUs decreased with an increase in $W_{PEG}$. Fig. 10 shows the SEM images of BWPU2 film surfaces degraded in PBS/lipase solution at different time intervals. Small cracks could be seen on the surface of the BWPU2 film after the first week of degradation. After the second week of degradation, some tiny holes appeared on the surfaces of the BWPU2 films. After 3 or 4 weeks of degradation, the holes on the surface of BWPU2 films gradually increased, both the diameter and depth of the holes increased, and some were cracked. In summary, BWPU had good biodegradability in PBS/lipase solution.

### 3.8 Comparison with literature work

Table 7 presents the comparisons between some key properties of BWPUs in this study with those of WPUs or PU reported in literature. By introducing a hydrophilic prepolymer containing

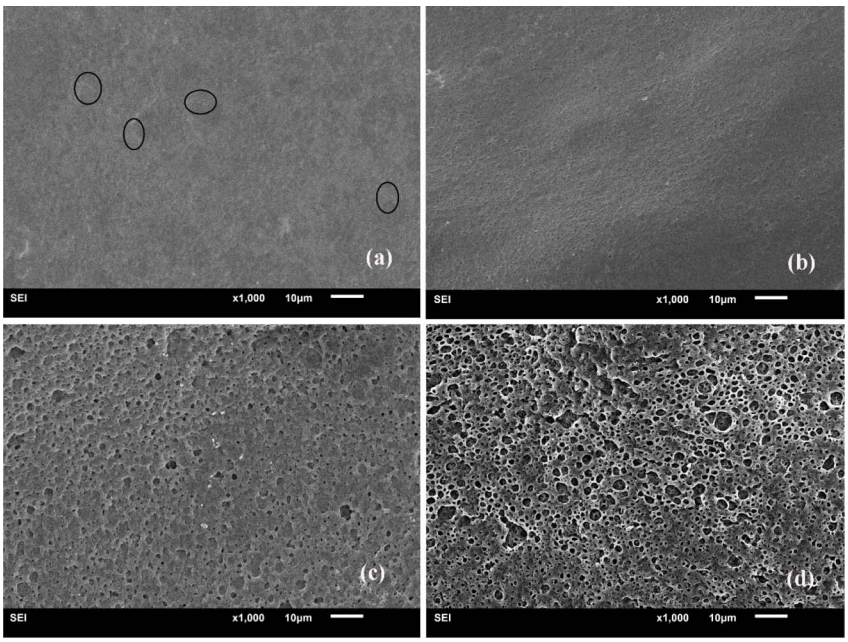


Fig. 10 SEM images of BWPU2 film surfaces after degradation in PBS/lipase solution after 1 week (a), 2 weeks (b), 3 weeks (c), and 4 weeks (d).

Table 7 Comparison of properties of PCL based WPUs or PUs with PEG

| Sample | Soft segments | Tensile strength (MPa) | Elongation at break (%) | Water absorption (%) | References |
|---|---|---|---|---|---|
| PEGCL-I-25_1 | PCL/PEG diblock | 5.1 | 20.6 | 35 | 36 |
| PEGCL-I-25_2 | PCL/PEG diblock | 19.9 | 836.6 | 25 | 36 |
| PU12 | PCL/PEG diblock | 3.6 | 425.4 | 92 | 54 |
| PEGPU33 | PCL/PEG diblock | 16.5 | 954.8 | — | 55 |
| PEGPU25 | PCL/PEG diblock | 10.2 | 816.0 | — | 55 |
| BPUR 50HS | PCL/PEG/PCL triblock | 20.0 | 260.0 | 16 | 56 |
| XEUP4 | PCL/PEG/glycidol | 1.2 | 132.1 | 21 | 57 |
| BWPU2 | PCL/PEG diblock | 56.8 | 827.1 | 18 | Our work |
| BWPU3 | PCL/PEG diblock | 53.4 | 921.2 | 32 | Our work |

PEG into WPU without using organic solvents and catalysts in the preparation, the comprehensive properties, especially the solid content and mechanical properties of PCL-based WPU be significantly improved. The WPU synthesized using PEG/PCL as the soft segment in literature[36,54–57] had maximum tensile strength only 20 MPa, while the BWPU2 and BWPU3 prepared in this study had tensile strengths as high as 56.8 MPa and 53.4 MPa, respectively. As compared with the organic solvent-based BPUR 50HS,[56] the water absorption of BWPU2 was slightly higher than that of BPUR 50HS, but lower than those of other water-based WPUs reported in literature.

## 4. Conclusions

Biodegradable BWPU was prepared without using organic solvents and catalysts by a special synthetic method, wherein a hydrophilic prepolymer was added during the preparation of BWPU prepolymer. Different amounts of PEG (0, 8 wt%, 16 wt%, 24 wt%, and 32 wt%) were introduced into the PCL-based WPU to improve the comprehensive properties of BWPUs. Results showed that the BWPUs containing PEG had higher solids content than the BWPU without PEG. The BWPU2 with 16% of PEG had the highest solids content of 53.1% and the smallest particle size and particle size distribution of 214.32 nm and 0.1, respectively. This was attributed to the special method of synthesis and optimal PEG content. The results also showed that the BWPU0 without PEG had a greater degree of phase separation than that of the BWPUs with PEG. Therefore, the introduction of PEG decreased the degree of phase separation of BWPUs, which affected the crystallization and dynamic mechanical properties of BWPUs. With an increase in PEG content, crystallinity decreased and the glass transition temperature of the hard segment decreased, whereas the glass transition temperature of the soft segment increased. The introduction of PEG significantly increased the tensile strength and Young's modulus of BWPU. BWPU2 had the highest tensile strength of 56.83 MPa, whereas BWPU0 had only 21.81 MPa. The hydrophilicity and surface energy of BWPU films increased with an increase in PEG content. In addition, the biodegradation experiment showed that BWPUs had good biodegradability. After degradation in PBS/lipase within 4 weeks, the mass losses from BWPU0 to BWPU4 were 6.3%, 4.3%, 3.5%, 2.6%, and 2.3%, respectively.

## Conflicts of interest

There are no conflicts to declare.

## Acknowledgements

This study was funded by applied basic research project of Science and Technology Department of Qinghai Province (Grant No. 2024-ZJ-779).

## References

1 A. B. Kutikov and J. Song, *ACS Biomater. Sci. Eng.*, 2015, **1**(7), 463–480.
2 S. Luo, K. Yang, Z. Zhong, X. j. Wu and T. B. Ren, *RSC Adv.*, 2018, **8**, 37765.
3 A. G. M. B. Mustayen, M. G. Rasul, X. Wang, M. A. Hazrat, M. I. Islam and M. Negnevitsky, *J. Energy Inst.*, 2023, **107**, 101198.
4 J. Rydz, K. Duale, H. Janeczek, W. Sikorska, A. Marcinkowski and M. Musioł, *Int. J. Mol. Sci.*, 2022, **23**(14), 7693.
5 J. T. Chen, H. X. Yang, Y. Qian, X. P. Ouyang, D. J. Yang, Y. X. Pang, L. Lei and X. Q. Qiu, *ACS Sustain. Chem. Eng.*, 2023, **11**(6), 2613–2622.
6 R. L. Shen, M. J. Long, C. D. Lei, L. M. Dong, G. P. Yu and J. T. Tang, *Chem. Eng. J.*, 2022, **433**, 134470.
7 L. Zhi, C. Q. Zhang, Z. Z. Liu, T. Liu, X. Y. Dou, Y. Q. Chen, R. X. Ou and Q. W. Wang, *Composites, Part B*, 2022, **230**, 109502.
8 A. Rahimi, A. Farhadian, L. Guo, E. Akbarinezhad, R. Sharifi, D. Iravani, A. A. Javidparvar, M. A. Deyab and M. A. Varfolomeev, *J. Ind. Eng. Chem.*, 2023, **123**(25), 170–186.
9 Z. H. Wu, X. Y. Zhang, S. M. Kang, Y. Liu, R. Bushra, J. Q. Guo, W. S. Zhu, M. R. Khan, Y. C. Jin and J. L. Song, *Ind. Crops Prod.*, 2023, **197**, 116512.
10 F. Naz, M. Zuber, K. M. Zia, M. Salman, J. Chakraborty, I. Nath and F. Verpoort, *Polym.*, 2018, **200**(15), 54–62.
11 S. K. Prajapati, A. Jain, A. Jain and S. Jain, *Eur. Polym. J.*, 2019, **120**, 109191.
12 S. Liu, Y. Y. Xie, L. D. Wang, C. X. Tai, D. Chen, D. Mu, Y. Y. Cui and B. Wang, *Neural Regener. Res.*, 2021, **16**(11), 2284–2292.
13 F. Yu, M. Li, Z. P. Yuan, F. Rao, X. X. Fang, B. G. Jiang, Y. Q. Wen and P. X. Zhang, *Int. J. Nanomed.*, 2018, **13**, 7845–7858.
14 T. Travinskaya, Yu. Savelyev and E. Mishchuk, *Polym. Degrad. Stab.*, 2014, **101**, 102–108.
15 Z. D. Dai, P. P. Jiang, W. X. Lou, P. B. Zhang, Y. M. Bao, X. W. Gao and J. L. Xia, *Eur. Polym. J.*, 2020, **139**, 109994.
16 T. J. Lee, S. H. Kwon and B. K. Kim, *Prog. Org. Coat.*, 2014, **77**, 1111–1116.
17 C. Denktaş, D. Y. Baysoy, A. Bozdoğan, H. S. Bozkurt, K. Bozkurt, O. Özdemir and M. Yilmaz, *J. Appl. Polym. Sci.*, 2022, **139**(18), 52086.
18 H. Tian, Z. Tang, X. Zhuang, X. Chen and X. Jing, *Prog. Polym. Sci.*, 2012, **37**, 237–280.
19 L. S. Nair and C. T. Laurencin, *Prog. Polym. Sci.*, 2007, **32**, 762–798.
20 G. E. Fawal, H. Hong, X. Mo and H. Wang, *J. Drug Delivery Sci. Technol.*, 2021, **63**, 102501.
21 F. Hajiali, S. Tajbakhsh and A. Shojaei, *Polym. Rev.*, 2018, **58**, 164–207.
22 A. Alcudia, B. Begines, P. Rodriguez-Lejarraga, V. Greyer, V. C. F. Godinho, E. Pajuelo and Y. Torres, *Colloid Polym. Sci.*, 2022, **48**, 100621.
23 P. Thiangpak and A. Rodchanarowan, *ACS Omega*, 2020, **5**, 25647–25654.
24 C. W. Ou, C. H. Su, U. S. Jeng and S. H. Hsu, *ACS Appl. Mater. Interfaces*, 2014, **6**, 5685–5694.
25 S. Cakić, I. Ristić, I. Krakovský, D. T. Stojiljković, P. Bělský and L. Kollová, *Mater. Chem. Phys.*, 2014, **144**(1–2), 31–40.

26 M. Kidwai, D. Bhatnagar and N. K. Mishra, *Green Chem. Lett. Rev.*, 2010, **3**, 55–59.
27 Y. Wang, S. Zhang, D. S. Benoit and J. Contr, *Release*, 2018, **287**, 58–66.
28 V. Srivastava, D. S. Chauhan, P. G. Joshi, V. Maruthapandian, A. A. Sorour and M. A. Quraishi, *ChemistrySelect*, 2018, **3**, 1990–1998.
29 F. Liu, C. X. Lu and T. Q. Sun, *Mater. Today Chem.*, 2022, **33**, 104716.
30 W. P. Liang, *Fundamentals of Emulsion Science and Technology*, Science Press, Beijing, 2001.
31 T. Y. Mao, H. Feng, J. R. Wu, M. Li, S. Luo, J. L. Chen, X. C. Wei, P. Liu and F. W. Xie, *Sustainable Mater. Technol.*, 2023, **36**, e00631.
32 L. H. Zhao, C. Y. Hong, C. H. Wang, J. W. Li, H. W. Ren and C. Zhou, *Prog. Org. Coat.*, 2023, **183**, 107765.
33 E. Princi, S. Vicini, K. Castro, D. Capitani, N. Proietti and L. Mannina, *Macromol. Chem. Phys.*, 2009, **210**, 879–889.
34 S. M. Cakić, I. S. Ristić, M. Marinović-Cincović and M. Špírková, *Int. J. Adhes. Adhes.*, 2013, **41**, 132–139.
35 C. C. Miao, Z. H. Li, K. Li, Y. N. Lv, X. C. Wu, X. J. Cao and Y. Wu, *Prog. Org. Coat.*, 2022, **165**, 106741.
36 S. Cometa, I. Bartolozzi, A. Corti, F. Chiellini, E. De Giglio and E. Chiellini, *Polym. Degrad. Stab.*, 2010, **95**, 2013–2021.
37 S. Mondal and J. L. Hu, *J. Membr. Sci.*, 2006, **276**, 16–22.
38 S. Mondal and J. L. Hu, *Polym. Int.*, 2006, **55**, 1013–1020.
39 M. Safari, J. Maiz, G. Shi, D. Juanes, G. Liu, D. Wang, C. Mijangos, A. Alegria and A. J. Müller, *Langmuir*, 2019, **35**, 15168–15179.
40 M. Irigoyen, A. Fernandez, A. Ruiz, F. Ruipérez and J. M. Matxain, *J. Org. Chem.*, 2019, **84**, 4200.
41 C. Chen, T. Zhang, X. Zhou, H. Lin, J. Z. Cui, X. H. Liu and H. B. Li, *Prog. Org. Coat.*, 2022, **167**, 106826.
42 S. P. Chen, W. Y. Zhang, Y. M. Ye, X. G. Ying, J. Y. Huang and X. Li, *Int. J. Adhes. Adhes.*, 2023, **125**, 103415.
43 H. Liang, Y. Li, S. Huang, K. Huang, X. Zeng, Q. Dong, C. Liu, P. Feng and C. Zhang, *ACS Sustain. Chem. Eng.*, 2019, **8**, 914–925.
44 H. Deng, F. Xie, H. Shi, Y. Li, S. Liu and C. Zhang, *Chem. Eng. J.*, 2022, **446**, 137124.
45 B. Chen, W. T. Xiong, C. L. Zhou, H. J. Zhang, X. Y. Pan, J. Peng, X. H. Luo, Z. H. Xie and Y. L. Liu, *Prog. Org. Coat.*, 2023, **183**, 107767.
46 S. P. Chen, W. Y. Zhang, Y. M. Ye, X. G. Ying, J. Y. Huang and X. Li, *Int. J. Adhes. Adhes.*, 2023, **125**, 103415.
47 Z. H. Sui, Y. P. Li, Z. A. Guo, Q. Zhang, Y. K. Xu and X. Zhao, *Prog. Org. Coat.*, 2022, **166**, 106783.
48 H. Q. Fu, C. B. Yan, W. Zhou and H. Huang, *J. Ind. Eng. Chem.*, 2014, **20**, 1623–1632.
49 L. Jiang, Y. L. Chen and C. P. Hu, *J. Coat. Technol. Res.*, 2007, **4**, 59–66.
50 D. E. Packham, *Int. J. Adhes. Adhes.*, 2003, **23**, 437–448.
51 Y. T. Han, Y. Z. Jiang, P. F. Tan, Y. Z. Zhang, Q. Z. Zhang, K. Li and L. Tan, *Prog. Org. Coat.*, 2022, **173**, 107219.
52 L. Liu, Z. B. Xia, C. B. Ou, L. Zhang and Z. Li, *Prog. Org. Coat.*, 2015, **88**, 155–163.
53 W. T. Xiong, B. Chen, H. J. Zhang, J. P. Peng, X. Y. Pan, M. Guo, X. H. Luo, C. L. Zhou and Y. L. Liu, *Prog. Org. Coat.*, 2023, **185**, 107895.
54 B. R. Barrioni, S. M. Carvalho, R. L. Oréfice, A. A. R. Oliveira and M. Magalhães Pereira, *Mater. Sci. Eng., C*, 2015, **52**, 22–30.
55 N. J. Song, X. J. Jiang, J. H. Lia, Y. P. Pang, J. S. Lia, H. Tan and Q. Fu, *Chin. J. Polym. Sci.*, 2013, **10**, 1451–1462.
56 A. P. Kishan, T. W. Wilems, S. M. Mohiuddin and E. M. Cosgriff-Hernandez, *ACS Biomater. Sci. Eng.*, 2017, **3**, 3493–3502.
57 H. Yeganeh a, M. M. Lakouraj and S. Jamshidi, *Eur. Polym. J.*, 2005, **41**, 2370–2379.